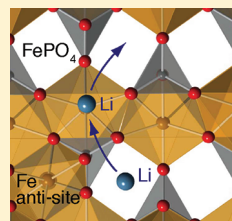


## Calculations of Li-Ion Diffusion in Olivine Phosphates

Gopi Krishna Phani Dathar, Daniel Sheppard, Keith J. Stevenson, and Graeme Henkelman\*

Department of Chemistry and Biochemistry, University of Texas at Austin, Austin, Texas 78712, United States

**ABSTRACT:** Kinetic pathways of Li-ion diffusion in olivine phosphates are calculated from density functional theory (DFT). Previously reported theoretical diffusion rates for Li ions and vacancies in defect-free crystalline  $\text{FePO}_4$  and  $\text{LiFePO}_4$  are six orders of magnitude faster than experimentally measured values. This discrepancy can be resolved by considering the different components of Li kinetics, including diffusion in the bulk, on the surface, in the presence of defects, and in varying local environments. Using DFT+U, we quantify each of these effects and determine that, while bulk diffusion is affected by strain and Li concentration, these are not significant enough to explain the slow diffusion observed in experiment. However, surface diffusion is observed to have high barriers, which could contribute to slow kinetics in nanostructured cathodes. Anti-site defects also provide a possible explanation for slow diffusion, but only for vacancy diffusion in  $\text{LiFePO}_4$ , which has a barrier of 0.71 eV, compared to 0.29 eV in defect-free channels. In  $\text{FePO}_4$ , a concerted Li-ion diffusion mechanism around the anti-site defect is found to have a low barrier of 0.35 eV, allowing for facile cross-channel diffusion at room temperature. The difference between Li-ion and vacancy diffusion is understood in terms of a favorable coordination between Li ions and localized electrons on Fe centers at the transition states for Li-ion hopping in  $\text{FePO}_4$ . Greater distances between vacancies and holes at the transition states for vacancy diffusion lead to higher diffusion barriers.



**KEYWORDS:** lithium ions, iron phosphate, diffusion, kinetics, anti-site defects, polarons

## INTRODUCTION

Olivine phosphates are widely researched cathode materials for Li-ion batteries, because of their cyclability and stability over a wide range of temperatures. Lithiated iron phosphate ( $\text{LiFePO}_4$ ), which was first reported by Padhi et al.,<sup>1</sup> has a theoretical specific charge capacity of 170 mAh/g and a  $\text{Fe}^{2+/3+}$  redox couple at 3.5 V.  $\text{LiFePO}_4$  has an olivine structure with corner-sharing  $\text{FeO}_6$  octahedra in the  $bc$ -plane,  $\langle 110 \rangle$ , and edge-sharing  $\text{LiO}_6$  octahedra stacked along the  $b$ -axis,  $\langle 010 \rangle$ . Li-ion diffusion in the lattice is uniaxial along the  $b$ -direction, where Li ions hop between octahedral sites via a tetrahedral hollow formed by the edge-sharing  $\text{LiO}_6$  octahedra. One-dimensional diffusion was first reported in theory<sup>2</sup> and later confirmed in experiments.<sup>3</sup>

$\text{LiFePO}_4$  is a promising material for use in cathodes but is limited by its low ionic and electronic conductivity. Both the lithiated and delithiated phases are wide-gap insulators that limit electronic conductivity to a hopping mechanism between Fe centers. Early studies by Franger et al. estimated Li diffusion in  $\text{LiFePO}_4$  at  $10^{-13}$ – $10^{-14}$   $\text{cm}^2/\text{s}$  and Li diffusion in  $\text{FePO}_4$  to be  $10^{-16}$   $\text{cm}^2/\text{s}$ .<sup>4,5</sup> The slow diffusion rate has been attributed to a variety of material properties including the two-phase coexistence ( $\text{Li}_x\text{FePO}_4$  and  $\text{Li}_{1-x}\text{FePO}_4$ ) during charge/discharge, the large miscibility gap between the end members at room temperature,<sup>6–8</sup> the unidimensionality of ionic diffusion,<sup>2,3</sup> and the phase transformation during lithiation.<sup>9,10</sup> Efforts to increase the conductivity include carbon coating, nanosizing,<sup>7,8</sup> off-stoichiometric synthesis,<sup>11</sup> and aliovalent ion doping.<sup>12</sup>

Improved charge/discharge kinetics in  $\text{LiFePO}_4$  particles has been observed after coating the particles with carbon.<sup>13,14</sup> It is believed that carbon coating restores the ordered phase of olivines, improves the interparticle connectivity, and increases electronic conductivity.<sup>15</sup> The effect of carbon coating on the

Li ion transport is not clear. Meethong et al.<sup>7</sup> reported improved charge/discharge kinetics in nanoparticles with shorter diffusion lengths and increased miscibility between the lithiated and unlithiated materials. A vanishing miscibility gap for particles <40 nm in size is reported,<sup>16</sup> and in studies of particles <50 nm in size, a solid solution is possible where phase boundaries cease to exist.<sup>17</sup>

Strain is reported to play a role in the kinetics of Li-ion transport. There are several models that explain the observed Li-ion transport and interface front propagation in  $\text{LiFePO}_4$  particles. These include the shrinking-core model,<sup>18</sup> the domino cascade model,<sup>19</sup> and a model for Li extraction at the biphasic interface.<sup>20</sup> The domino-cascade model asserts that delithiation is fast, following nucleation of one phase in the other, which explains why particles are either fully lithiated or fully delithiated. Chen et al.<sup>20</sup> reported the existence of two phases during lithiation and delithiation involving a first-order phase transformation. The movement of a phase boundary is observed parallel to the  $bc$ -plane. The two phases, lithiated and delithiated, differ in lattice volume, so strain is induced at the phase boundary. The facile extraction of Li ions at the interface is reported to contribute to the improvement in the electrochemical activity of  $\text{LiFePO}_4$  nanoparticles.<sup>20</sup> This model was later supported by spectroscopic studies of  $\text{LiFePO}_4$  particles.<sup>21</sup> A recent model based on a modified Cahn–Hilliard equation also supports the domino-cascade model in the low current limit.<sup>22</sup>

Theoretical studies report energy barriers for Li-ion transport in the bulk of iron phosphate and vacancy diffusion in the

Received: June 7, 2011

Revised: August 3, 2011

Published: August 18, 2011

lithiated phase are 0.18 and 0.27 eV, respectively.<sup>2</sup> These density functional theory (DFT) calculations fail to localize the electrons from the Li ions on Fe centers. Later studies<sup>23,24</sup> report localized electrons at the transition-metal centers result in stronger Li-ion binding in the material. The localized electrons, which induce polaronic distortions in the crystal, explain the discrepancies in the theoretical and experimental band gap and redox potential of the Fe<sup>2+/3+</sup> couple. The strong binding of localized polarons in this material — 0.37 eV in FePO<sub>4</sub> and 0.50 eV in LiFePO<sub>4</sub> — contribute to the high barrier for Li-ion transport.<sup>25,26</sup>

Calculations show that anti-site defects are the most favorable intrinsic defect in LiFePO<sub>4</sub>.<sup>27,28</sup> Recently, high-angle annular dark-field scanning transmission electron microscopy was used to observe disordered arrangements of Fe in Li sites.<sup>29</sup> These anti-site defects are reported to block Li-ion diffusion in the channels and lead to structural instability. The effect of particle size on Li-ion and vacancy diffusion from theoretical studies report that anti-site defects present in the channels in macrosized particles result in slower diffusion, compared to their nanosized counterparts.<sup>30</sup>

These research efforts provide insight into the kinetics of Li-ion diffusion in FePO<sub>4</sub> but there is no consensus on the rate-limiting mechanisms of charging for the bulk material and nanoparticles. The diffusivity of Li is reported from various experimental studies in the range of 10<sup>-11</sup>–10<sup>-17</sup> cm<sup>2</sup>/s.<sup>4,5,7,31–36</sup> These studies report that the variation in diffusivity arises from the state of charge, particle size, quality of carbon coating, synthesis procedures, and other experimental details. Another puzzle is that theoretical studies predict low energy barriers, corresponding to fast bulk Li-ion diffusion (10<sup>-8</sup>–10<sup>-9</sup> cm<sup>2</sup>/s).<sup>2,37</sup> However, the overall Li-ion transport in devices has contributions besides bulk diffusion in defect-free FePO<sub>4</sub>. In this paper, we calculate the energy barriers for Li-ion diffusion in bulk, on the surface, and in the presence of defects using DFT+U. The effect of localized electrons, occupied or vacant neighboring Li sites, and change in channel dimensions on diffusion are studied. Energy barriers relevant to the overall diffusion kinetics are then discussed.

## COMPUTATIONAL METHODS

Total energy calculations were performed using DFT+U, as implemented in the Vienna Ab-Initio Simulation Package (VASP).<sup>38,39</sup> The initial structures for LiFePO<sub>4</sub> and FePO<sub>4</sub> were obtained from the ICSD Database. Optimized structures were calculated using the PW91 functional<sup>40</sup> with the VWN interpolation formula<sup>41</sup> and projector-augmented-wave<sup>42</sup>-based pseudo-potentials. The DFT+U method proposed by Dudarev et al.<sup>43</sup> was used to model electrons on the transition-metal centers in FePO<sub>4</sub>. This method has been shown to localize polarons on Fe centers using appropriate on-site corrections.<sup>25,26,37</sup> The on-site Hubbard term (*U*) was set to best reproduce the experimental electronic band gap with a difference (defined as  $U_{\text{eff}} = U - J$ ) of 4.3 eV.

All calculations were spin-polarized, using a plane-wave cutoff of 500 eV and a *k*-point mesh with a spacing of <0.03 Å<sup>-1</sup>. Ferromagnetic spin ordering was initialized on the Fe ions. Geometry optimizations were considered converged when the force on each atom was <5 meV/Å. The reference energy for Li was calculated from its metallic state. Supercells containing 1 × 3 × 2 unit cells were used. The lattice parameters of cells containing an anti-site defect were optimized and then held fixed in subsequent calculations of binding energies and barriers.

Minimum energy pathways and saddle points connecting Li-ion binding sites were calculated with the climbing-image nudged elastic

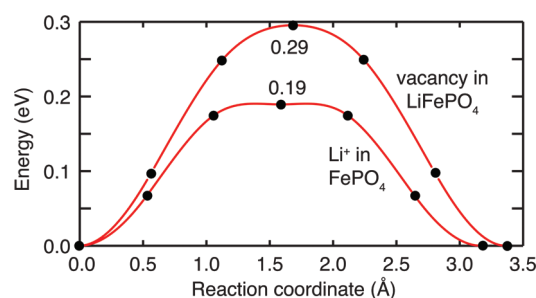


**Figure 1.** Minimum energy paths for Li-ion hopping in FePO<sub>4</sub> and Li-vacancy hopping in LiFePO<sub>4</sub>.

band method.<sup>44</sup> Supercells containing 1 × 3 × 2 unit cells were used to determine energy barriers for diffusion. The size of the supercell was considered converged when energy barriers changed by <0.02 eV. Minimum energy configurations corresponding to the initial and final states were determined by trying various configurations of the electrons localized on the Fe centers. All ions were relaxed for calculations of the minimum energy pathways, and the lattice parameters were held fixed.

Surfaces were built by cleaving the optimized bulk crystal to expose the *ac*-plane. The surface termination exposing this <010> face is reported to have a lower surface energy, compared to other low-indexed surfaces, and dominates the surface of particles under equilibrium (via the Wulff construction) and nonequilibrium conditions.<sup>45</sup> This surface also has Li-ion diffusion channels running perpendicular to the *ac*-plane and are suited for calculations of diffusion across channels, as well as into the subsurface and bulk. A vacuum space of 10 Å was used to separate periodic images in the surface model. The number of layers used to represent the surface was chosen so that the change in the binding of Li ions on the surface decreased to <0.02 eV.

## RESULTS

**Bulk Diffusion.** The rate of Li-ion diffusion was calculated from the difference in energy between the saddle point along the hopping pathway and the initial minimum. The minimum energy state is the configuration with a Li ion (vacancy) in one of the octahedral sites in the lattice with a vacant (filled) adjacent octahedral site in FePO<sub>4</sub> (LiFePO<sub>4</sub>). The energy barriers for Li-ion and vacancy diffusion are calculated to be 0.19 and 0.29 eV. These barriers are shown in Figure 1 and are summarized with those of other diffusion mechanisms later in Table 1. The DFT+U calculations are significantly different from DFT, in terms of binding energies and band gaps.<sup>23,24</sup> Remarkably, the DFT+U diffusion barriers are similar to those calculated with DFT by Morgan et al.,<sup>2</sup> suggesting a cancellation of errors between the energy of minima and transition states. As we discuss in the next section, however, lower barriers can be found if electrons localized with DFT+U are able to move in a reaction and better coordinate charge carriers at the transition state.

**Localized Electrons.** In iron phosphate, electrons localize on Fe centers and induce polaronic distortions in the coordinating O atoms. Since there are many Fe centers in the lattice near a Li ion (see Figure 2), more than one electronic state is possible. The configuration with the lowest energy has the electron closest to the Li ion. However, the closest Fe center can change along diffusion pathways. In Figure 1, the electron remains localized on the Fe site nearest to the Li ion in the reactant (and product) state for diffusion (Fe1 in Figure 2). Also shown in Figure 2 is a diffusion path in which the electron is localized on the out-of-plane Fe center, which is closest to the Li ion at the transition

Table 1. Energy Barriers for Li-Ion (Vacancy) Hopping in FePO<sub>4</sub> (LiFePO<sub>4</sub>)<sup>a</sup>

	Li Ion in FePO <sub>4</sub>		Vacancy in LiFePO <sub>4</sub>	
	energy barrier (eV)	diffusivity (cm <sup>2</sup> /s)	energy barrier (eV)	diffusivity (cm <sup>2</sup> /s)
bulk diffusion	0.19	$6 \times 10^{-7}$	0.29	$1 \times 10^{-8}$
polaron hopping	0.13, 0.19	$6 \times 10^{-6}$	0.29, 0.51	$1 \times 10^{-8}$
occupied/vacant neighbors	0.12–0.30	$9 \times 10^{-6} - 9 \times 10^{-9}$	0.25–0.44	$6 \times 10^{-8} - 4 \times 10^{-11}$
lattice strain	0.19–0.30	$6 \times 10^{-7} - 9 \times 10^{-9}$	0.29–0.20	$1 \times 10^{-8} - 4 \times 10^{-7}$
cross-channel diffusion	0.35	$1 \times 10^{-9}$	0.71	$1 \times 10^{-15}$
surface diffusion	0.52, 0.77	$9 \times 10^{-12}, 6 \times 10^{-16}$		

<sup>a</sup> Diffusivity is calculated using the Einstein–Smoluchowski relation:  $D = \frac{1}{2} \Gamma d^2$ , where  $\Gamma$  is the rate ( $\nu = 2 \times 10^{12}$ /s and  $T = 300$  K) to hop between sites and  $d = 3.07$  Å is the distance between sites. For surface diffusion,  $d = 6.63$  Å.

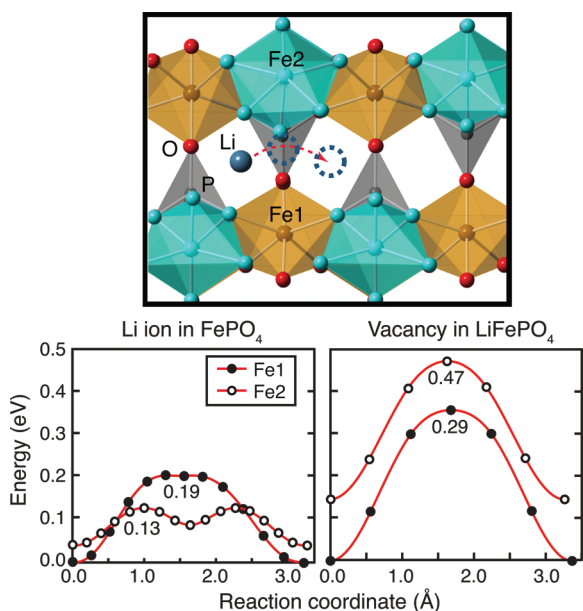


Figure 2. (a) Li-ion diffusion in FePO<sub>4</sub> with the electron localized on iron site Fe1, in-plane with the diffusion path, or on the out-of-plane Fe2 site. (b) Minimum energy paths for Li-ion and vacancy diffusion with the localized countercharge on the specified iron site.

state (Fe2). In the first path, the end points are stabilized and the barrier is 0.19 eV. In the second, the saddle geometry is stabilized by 0.1 eV to give an intermediate minimum along the path. The activation energy of 0.13 eV for the second pathway is the barrier to enter this intermediate minimum.

In LiFePO<sub>4</sub>, the energy of the transition state for vacancy hopping is increased from 0.29 eV to 0.47 eV when the hole is moved from an in-plane center to an out-of-plane Fe center. The difference between Li-ion and vacancy diffusion is due to the relative signs of the charge carriers; in FePO<sub>4</sub>, the Coulombic attraction between the electron and the Li ion reduces the energy barrier, whereas in LiFePO<sub>4</sub>, the Coulombic repulsion between the localized hole and the Li ion at the saddle results in a higher energy barrier.

**Neighbor Interactions.** Li ions in LiFePO<sub>4</sub> form LiO<sub>6</sub> octahedra, which share corners along the *b*-axis. These corner-sharing octahedra are separated by vacant tetrahedra, so no atoms separate Li ions in adjacent sites along this direction to screen the electrostatic interaction. Hence, the movement of Li ions is correlated in the one-dimensional channel. Along the *a*-axis, Li

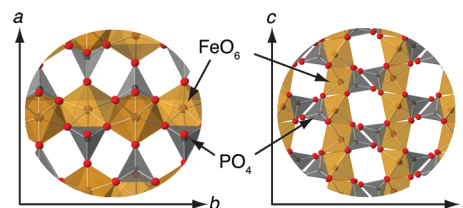


Figure 3. Stacked Li-ion diffusion channels in FePO<sub>4</sub> in (a) the *bc*-plane and (b) the *ac*-plane.

ions are separated by FeO<sub>6</sub> octahedra. The LiO<sub>6</sub> octahedra in the same channel share four O atoms with two LiO<sub>6</sub> octahedra in adjacent channels. When the octahedral site is occupied in one channel, the structure of the sites in the adjacent channels along the *a*-axis is affected. Along the *c*-axis, the correlation is less pronounced, since the two LiO<sub>6</sub> octahedron do not share O atoms. Thus, the Li ion in an octahedral site affects a total of six neighboring sites: two in the same channel along the *b*-axis and four in adjacent channels parallel to the *ac*-plane.

Our reference to understand neighbor interactions on diffusion are the hopping barriers of 0.19 and 0.29 eV for isolated Li ions and vacancies. Occupied first neighbors (vacant neighboring sites for vacancy diffusion) result in decreased energy barriers for two reasons: (i) repulsion between carriers when present in the same channel and (ii) partially relaxed shared LiO<sub>6</sub> octahedra and the attraction between Li ion (vacancy) and localized electron (hole) on the out-of-plane Fe sites. The energy barrier is not significantly affected by second neighbors, with changes of <0.01 eV. In FePO<sub>4</sub>, the highest computed barrier of 0.30 eV is when a Li ion diffuses toward a vacant site with completely filled adjacent sites. The vacancies in LiFePO<sub>4</sub> behave similarly to the Li ions in LiFePO<sub>4</sub>. The highest value of 0.44 eV results when the vacancy diffuses toward a filled site adjacent to other vacant sites.

**Lattice Strain.** The volume of FePO<sub>4</sub> increases upon lithiation by 5%. The electrons associated with the Li ions are transferred to the closest FeO<sub>6</sub> octahedra, increasing the Fe–O bond lengths. The channels for Li-ion diffusion run along the *b*-lattice direction, stacked in ABAB fashion along the *a*-lattice direction, and in AAA fashion along the *c*-lattice direction (see Figure 3). This change in the lattice dimensions induces strain fields in the *ac*-plane, making Li-ion diffusion more facile at the interface.

Two sets of calculations are done to study the effect of changes in lattice dimensions. The initial structure in the first set of calculations is an optimized FePO<sub>4</sub> lattice with one Li ion. The

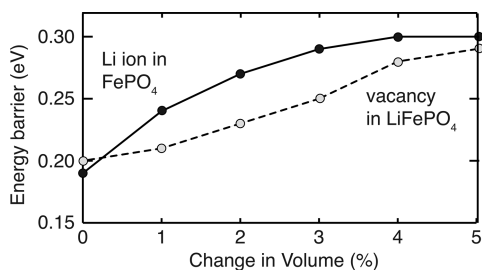


**Figure 4.** Change in the energy barrier for Li-ion and vacancy diffusion with lattice volume, scaled between that of FePO<sub>4</sub> and LiFePO<sub>4</sub>.

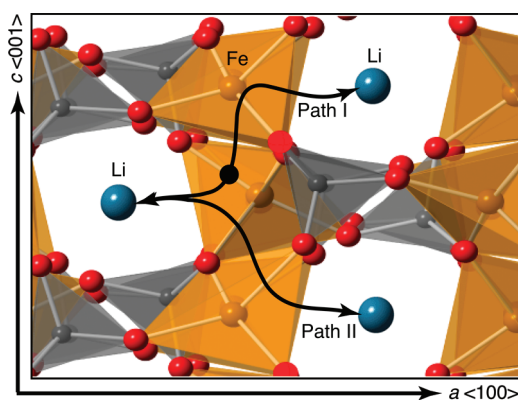


**Figure 5.** Li-ion diffusion pathways on the FePO<sub>4</sub> surface.

energy barrier to hop between the octahedral sites is calculated as a function of lattice parameters, using five linear increments between those of FePO<sub>4</sub> and LiFePO<sub>4</sub>. In the second set of calculations, the procedure is reversed, starting with a vacancy in LiFePO<sub>4</sub>.

The diffusion barrier for Li in the FePO<sub>4</sub> lattice increases with lattice expansion and the vacancy diffusion barrier decreases with compression of the channel dimensions (see Figure 4). This result is somewhat surprising, because intuition would suggest that an expansion of the lattice would increase diffusion rates. Instead, Li at their minima are stabilized with lattice expansion to a greater extent than at the transition state, making diffusion faster in FePO<sub>4</sub> than LiFePO<sub>4</sub>. Also, once the delithiation process is started, the channels start to shrink making diffusion favorable in adjacent channels. A systematic study of this effect, such as that which was done for Li<sub>2</sub>MnO<sub>4</sub> spinel,<sup>46</sup> is required to understand the origin of the trend.

**Surface Diffusion.** Li-ion diffusion on the FePO<sub>4</sub> surface is calculated in the dilute Li limit. Our calculations show Li ions prefer to sit at channel entrances with the electrons localized at the nearest Fe centers. Two types of calculations are done to determine Li-ion transport on the surface: diffusion of Li ions between channels on the surface and from the surface into the bulk. Paths found for diffusion between channels on the surface are shown in Figure 5.

Two such paths are found connecting the channels stacked along  $\langle 100 \rangle$ . The channels along  $\langle 001 \rangle$  are separated by PO<sub>4</sub><sup>3-</sup> tetrahedra; no direct path was found connecting these channels. Path I, with a barrier of 0.52 eV, curves around the out-of-plane oxygen from the nearest PO<sub>4</sub><sup>3-</sup> tetrahedron and settles into a shallow intermediate minimum (see the black dot in Figure 5),

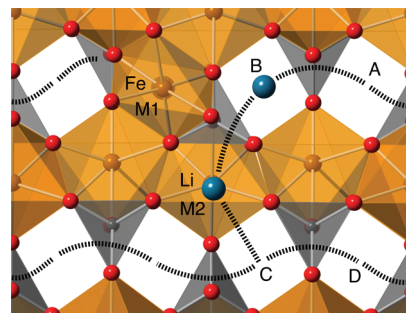


**Figure 6.** For the anti-site defect shown, Fe sits in the channel at site M1 and Li sits in the FePO<sub>4</sub> lattice at site M2. Dashed lines represent the diffusion pathways for Li ions in the lattice.

before reaching the entrance to the neighboring channel. Path II, with a barrier of 0.77 eV, is also curved around the O atoms in the nearest FeO<sub>6</sub> octahedra. In order to access all channel entrances on the surface, both barriers must be crossed.

Li ions readily diffuse into the subsurface crossing a barrier of 0.13 eV. Li ions bind more strongly at subsurface sites by 0.20 eV, making the reverse barrier higher than that for diffusion into the bulk. Since surface diffusion has a higher activation energy than bulk diffusion, the ability of Li to reach channel entrances is a possible rate-limiting step in charge/discharge kinetics.

**Anti-site Defects.** Anti-site defects commonly arise in olivines during the synthesis process. They are characterized by an exchange of Li and Fe in the lattice. In Figure 6, Fe sits in the channel at site M1 and Li sits in the FePO<sub>4</sub> framework at site M2. It costs 0.55 eV to form the anti-site defect in LiFePO<sub>4</sub>. Our calculated anti-site defect formation energy compares well with the previously reported values from both DFT+U and empirical potentials.<sup>27,28,30,47</sup> Li-ion and vacancy binding energies and diffusion barriers in the presence of the anti-site defect in FePO<sub>4</sub> and LiFePO<sub>4</sub> are also calculated.

The Li ion in the anti-site defect is bound more strongly than in a defect-free channel. Taking the binding in a defect-free channel (3.25 eV) as our reference, Li binds more strongly at the M2 site (by 2.2 eV) and at the A and D sites around the defect (by 0.80 eV). Similarly, in LiFePO<sub>4</sub>, the energy required to create a vacancy at the M2 site is higher (by 0.72 eV) than in a defect-free channel (3.74 eV). The strong binding of Li at the M2 site means that the M2 site will be occupied before neighboring channel sites.

Previous calculations using DFT report a barrier of 0.49 eV for Li-ion cross-channel diffusion in FePO<sub>4</sub>.<sup>30</sup> The rate-limiting step for this process is moving a Li ion from site M2 to the B or C site. However, the DFT+U calculations show that a single Li ion is unstable in the B and C sites and spontaneously moves to the M2 site. The A and D sites are determined to be metastable, with the M2 site being favored by 1.4 eV. The barrier to escape from the M2 site to the A or D site is high (1.6 eV), compared to the reverse barrier (0.2 eV) and to diffusion in the channel (0.19 eV). The strong binding of Li at the M2 site, as shown in the energy landscape in Figure 7a, makes it clear that the anti-site Li will not diffuse away from the defect. The qualitative difference between the DFT and DFT+U calculations is that the electron from Li is delocalized with DFT and localized on the channel Fe site with DFT+U. The Li ion at the M2 site is strongly favored with DFT+U, and any further separation from the electron at the M1 site results in a high Coulombic energy cost.

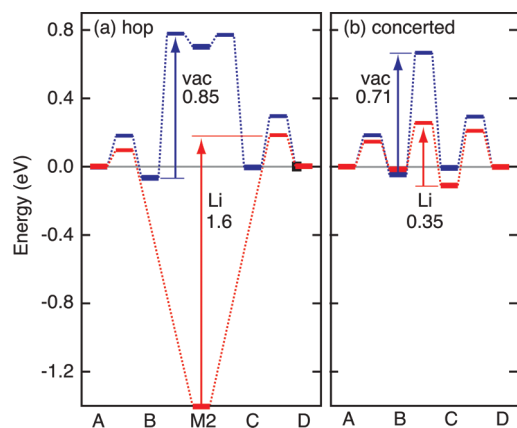


**Figure 7.** Energy landscape for diffusion around the defect resulting in cross-channel diffusion of Li ions (red) and vacancies (blue). Cross-channel diffusion of Li ions and vacancies via (a) single Li-ion/vacancy hopping and (b) concerted diffusion of Li ions, so that the M2 site is always occupied. Overall barriers for cross-channel diffusion are indicated. The sites labels are as given in Figure 6.

If the anti-site Li ion is trapped at the M2 site, a second Li ion can occupy the B or C sites. In this case, a concerted diffusion of Li ions, from the B site to the C site via the M2 site, is possible and has an energy barrier of 0.27 eV, with a reverse barrier of 0.35 eV. The barrier to diffuse away from the defect, from the B site to the A site and from the C site to the D site, are 0.21 and 0.33 eV, respectively, as shown in Figure 7b. Remarkably, an anti-site defect does not significantly slow down Li-ion diffusion, as has been reported previously; it also allows facile diffusion between channels. Concerted cross-channel diffusion is possible because the M2 site remains occupied and acts as a persistent charge donor for the anti-site Fe at the M1 site.

The barriers for a vacancy to hop from the B and C sites to the M2 site in  $\text{LiFePO}_4$  are calculated as 0.85 and 0.75 eV, respectively. Cross-channel vacancy diffusion from the B site to the C site, involving the concerted diffusion of Li ions via the M2 site, has an energy barrier of 0.71 eV, which is slightly lower than that for isolated vacancy diffusion. The cross-channel diffusion of vacancies in  $\text{LiFePO}_4$  remains significantly slower than Li ions in  $\text{FePO}_4$ . The energy landscape for these concerted mechanisms is shown in Figure 7b.

The low energy barrier for concerted cross-channel Li-ion diffusion in  $\text{FePO}_4$ , compared to vacancy diffusion in  $\text{LiFePO}_4$ , can be attributed to differences in the distances between the migrating species (Li ion or vacancy) and the corresponding localized counter-charge (electron or hole). Figure 8 shows the distances between Li ions/vacancies and the counter charges on nearby Fe sites for cross-channel diffusion around an anti-site defect. The two electrons associated with the Li ions in  $\text{FePO}_4$  localize on  $\text{Fe}^{2+}$  centers: one in the channel and the other adjacent to it (see Figure 8a). At the initial state, the two Li ions at the B and M2 sites are 3.23 and 3.34 Å, respectively, from the electron at the M1 site in the channel. At the transition state, the distances are similar: 3.19 and 4.60 Å. In  $\text{LiFePO}_4$ , the distance between the vacancy at the M2 site and the localized hole at the neighboring  $\text{Fe}^{3+}$  (see Figure 8b) is 3.28 Å, whereas at the transition state, the distances between the localized hole and two half vacancies are 3.28 and 8.51 Å. The energetic cost of separating charge explains the high barrier for vacancy diffusion between channels (0.71 eV), compared to Li ions (0.35 eV).

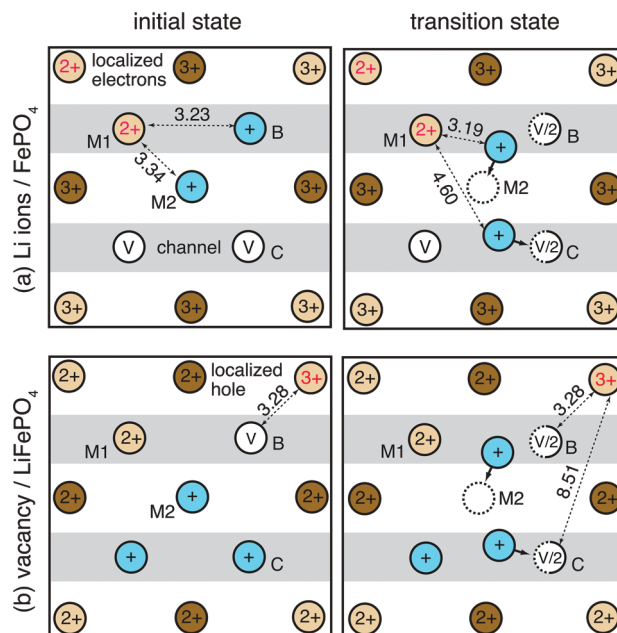


**Figure 8.** Distances between charged species for the initial state of (a) concerted Li-ion diffusion and (b) vacancy diffusion from an anti-site defect in  $\text{FePO}_4$  and  $\text{LiFePO}_4$ , as well as at the corresponding transition states. The sites labels are as given in Figure 6.

## DISCUSSION

The rate of Li-ion diffusion in bulk iron phosphate calculated from first principles is much faster than that observed in experiment. However, the overall diffusion in the material has different components, including diffusion in the bulk, in varying local environment, on the surface, and in the presence of defects. The diffusivity of carriers in iron phosphate is reported to be between  $10^{-12}$  and  $10^{-17}$   $\text{cm}^2/\text{s}$ , depending on the state of charge in the material. These diffusivity values translate to energy barriers in the range of 0.45–0.80 eV. Hence, identifying the rate-limiting diffusion phenomenon can provide insight into the function of the material. Our calculations of the barriers and diffusivities of the different components are summarized in Table 1.

The effects of different local environments, in terms of Li-ion and vacancy ordering, as well as sites for localized electrons, the energy barriers of Li-ion diffusion in bulk  $\text{FePO}_4$  and vacancy diffusion in  $\text{LiFePO}_4$ , vary in the range of 0.12–0.44 eV. The difference between measured and calculated diffusivity values cannot be solely addressed by these variations in bulk diffusion. The calculated barriers for surface diffusion, from 0.52–0.77 eV, are consistent with experiment and, in some cases, particularly when there is poor connectivity to the electrolyte, could play a role in limiting charge/discharge rates.

Perhaps the most likely cause for the observed slow Li-ion diffusion in olivine phosphates is the presence of anti-site defects. While it has been generally assumed that anti-site defects simply block channels, we find that a concerted diffusion mechanism around the anti-site defect is facile for Li ions in  $\text{FePO}_4$  and activated for vacancies in  $\text{LiFePO}_4$ . These mechanisms provide a range of barriers in the range of 0.35–0.71 eV, which is consistent with the range of barriers determined from experiment. An experimental signature predicted by these calculations would be fast isotropic diffusion of Li in  $\text{FePO}_4$  in a large crystal

that contains anti-site defects, and slow anisotropic diffusion of vacancies along the channels in LiFePO<sub>4</sub>.

## AUTHOR INFORMATION

### Corresponding Author

\*E-mail: henkelman@mail.utexas.edu.

## ACKNOWLEDGMENT

This work is supported as part of the program “Understanding Charge Separation and Transfer at Interfaces in Energy Materials (EFRC:CST)” an Energy Frontier Research Center funded by the U.S. Department of Energy, Office of Science, Office of Basic Energy Sciences (under Award No. DE-SC0001091). Computational resources from NERSC and the Texas Advanced Computing Center are acknowledged. We are grateful to Zachary Pozun for a critical reading of the manuscript.

## REFERENCES

- (1) Padhi, A. K.; Nanjundaswamy, K. S.; Goodenough, J. B. *J. Electrochem. Soc.* **1997**, *144*, 1188–1194.
- (2) Morgan, D.; Van der Ven, A.; Ceder, G. *Electrochem. Solid-State Lett.* **2004**, *7*, A30–A32.
- (3) Nishimura, S.; Kobayashi, G.; Ohoyama, K.; Kanno, R.; Yashima, M.; Yamada, A. *Nature Mat.* **2008**, *7*, 707–711.
- (4) Franger, S.; Le Cras, F.; Bourbon, C.; Rouault, H. *Electrochem. Solid-State Lett.* **2002**, *5*, A231–A233.
- (5) Prossini, P. P.; Lisi, M.; Zane, D.; Pasquali, M. *Solid State Ionics* **2002**, *148*, 45–51.
- (6) Yamada, A.; Koizumi, H.; ichi Nishimura, S.; Sonoyama, N.; Kanno, R.; Yonemura, M.; Nakamura, T.; Kobayashi, Y. *Nature Mat.* **2006**, *5*, 357–360.
- (7) Meethong, N.; Huang, H.-Y. S.; Carter, W. C.; Chiang, Y.-M. *Electrochem. Solid-State Lett.* **2007**, *10*, A134–A138.
- (8) Delacourt, C.; Poizot, P.; Levasseur, S.; Masquelier, C. *Electrochem. Solid-State Lett.* **2006**, *9*, A352–A355.
- (9) Yamada, A.; Koizumi, H.; Sonoyama, N.; Kanno, R. *Electrochem. Solid-State Lett.* **2005**, *8*, A409–A413.
- (10) Zhou, F.; Maxisch, T.; Ceder, G. *Phys. Rev. Lett.* **2006**, *97*, 155704.
- (11) Kang, B.; Ceder, G. *Nature* **2009**, *458*, 190–193.
- (12) Meethong, N.; Kao, Y.-H.; Speakman, S. A.; Chiang, Y.-M. *Adv. Funct. Mater.* **2009**, *19*, 1060–1070.
- (13) Ravet, N.; Chouinard, Y.; Magnan, J. F.; Besner, S.; Gauthier, M.; Armand, M. *J. Power Sources* **2001**, *97–98*, S03–S07.
- (14) Huang, H.; Yin, S.-C.; Nazar, L. F. *Electrochem. Solid-State Lett.* **2001**, *4*, A170–A172.
- (15) Julien, C. M.; Mauger, A.; Zaghbi, K. *J. Mater. Chem.* **2011**, *21*, 9955–9968.
- (16) Gibot, P.; Casas-Cabanas, M.; Laffont, L.; Levasseur, S.; Carlach, P.; Hamelet, S.; Tarascon, J.-M.; Masquelier, C. *Nat. Mater.* **2008**, *7*, 741–747.
- (17) Ramana, C. V.; Mauger, A.; Gendron, F.; Julien, C. M.; Zaghbi, K. *J. Power Sources* **2009**, *187*, S55–S64.
- (18) Srinivasan, V.; Newman, J. *J. Electrochem. Soc.* **2004**, *151*, A1517–A1529.
- (19) Delmas, C.; Maccario, M.; Croguennec, L.; Le Cras, F.; Weill, F. *Nature Mat.* **2008**, *7*, 665–671.
- (20) Chen, G.; Song, X.; Richardson, T. J. *Electrochem. Solid-State Lett.* **2006**, *9*, A295–A298.
- (21) Laffont, L.; Delacourt, C.; Gibot, P.; Wu, M. Y.; Kooyman, P.; Masquelier, C.; Tarascon, J. M. *Chem. Mater.* **2006**, *18*, 5520–5529.
- (22) Singh, G. K.; Ceder, G.; Bazant, M. Z. *Electrochim. Acta* **2008**, *53*, 7599–7613.
- (23) Zhou, F.; Cococcioni, M.; Marianetti, C. A.; Morgan, D.; Ceder, G. *Phys. Rev. B* **2004**, *70*, 235121.
- (24) Zhou, F.; Cococcioni, M.; Kang, K.; Ceder, G. *Electrochem. Commun.* **2004**, *6*, 1144–1148.
- (25) Maxisch, T.; Zhou, F.; Ceder, G. *Phys. Rev. B* **2006**, *73*, 104301.
- (26) Ellis, B.; Perry, L. K.; Ryan, D. H.; Nazar, L. F. *J. Am. Chem. Soc.* **2006**, *128*, 11416–11422.
- (27) Fisher, C. A. J.; Hart Prieto, V. M.; Islam, M. S. *Chem. Mater.* **2008**, *20*, 5907–5915.
- (28) Islam, M. S.; Driscoll, D. J.; Fisher, C. A. J.; Slater, P. R. *Chem. Mater.* **2005**, *17*, 5085–5092.
- (29) Chung, S.-Y.; Choi, S.-Y.; Yamamoto, T.; Ikuhara, Y. *Phys. Rev. Lett.* **2008**, *100*, 125502.
- (30) Malik, R.; Burch, D.; Bazant, M.; Ceder, G. *Nano Lett.* **2010**, *10*, 4123–4127.
- (31) Tang, K.; Yu, X.; Sun, J.; Li, H.; Huang, X. *Electrochim. Acta* **2011**, *56*, 4869–4875.
- (32) Amin, R.; Balaya, P.; Maier, J. *Electrochem. Solid-State Lett.* **2007**, *10*, A13–A16.
- (33) Amin, R.; Maier, J.; Balaya, P.; Chen, D. P.; Lin, C. T. *Solid State Ionics* **2008**, *179*, 1683–1687.
- (34) Whittingham, M. S.; Song, Y.; Lutta, S.; Zavalij, P. Y.; Chernova, N. A. *J. Mater. Chem.* **2005**, *15*, 3362–3379.
- (35) Wang, C.; Hong, J. *Electrochem. Solid-State Lett.* **2007**, *10*, A65–A69.
- (36) Churikov, A. V.; Ivanishchev, A. V.; Ivanishcheva, I. A.; Sycheva, V. O.; Khasanova, N. R.; Antipov, E. V. *Electrochim. Acta* **2010**, *55*, 2939–2950.
- (37) Ong, S. P.; Chevrier, V. L.; Ceder, G. *Phys. Rev. B* **2011**, *83*, 075112.
- (38) Kresse, G.; Furthmüller, J. *Comput. Mater. Sci.* **1996**, *6*, 15.
- (39) Kresse, G.; Furthmüller, J. *Phys. Rev. B* **1996**, *54*, 11169.
- (40) Perdew, J. P.; Wang, Y. *Phys. Rev. B* **1992**, *45*, 13244–13249.
- (41) Vosko, S. H.; Wilk, L.; Nusair, M. *Can. J. Phys.* **1980**, *58*, 1200–1211.
- (42) Blöchl, P. E. *Phys. Rev. B* **1994**, *50*, 17953.
- (43) Dudarev, S. L.; Botton, G. A.; Savrasov, S. Y.; Humphreys, C. J.; Sutton, A. P. *Phys. Rev. B* **1998**, *57*, 1505–1509.
- (44) Henkelman, G.; Uberuaga, B. P.; Jónsson, H. *J. Chem. Phys.* **2000**, *113*, 9901–9904.
- (45) Wang, L.; Zhou, F.; Meng, Y. S.; Ceder, G. *Phys. Rev. B* **2007**, *76*, 165435.
- (46) Xu, B.; Meng, S. *J. Power Sources* **2010**, *195*, 4971–4976.
- (47) Zhang, H.; Tang, Y.; Shen, J.; Xin, X.; Cui, L.; Chen, L.; Ouyang, C.; Shi, S.; Chen, L. *Appl. Phys. A: Mater. Sci. Process.* **2011**, *104* (2), 529–537.